**Title: Proximity Labeling Expansion Microscopy (PL-ExM) resolves structure of the interactome**

**Authors:** Sohyeon Park[1], Xiaorong Wang[2], Xiangpeng Li[3], Xiao Huang[4], Katie C. Fong[5,6], Clinton Yu[2], Arthur A. Tran[7], Lorenzo Scipioni[8,9], Zhipeng Dai[5], Lan Huang[2], Xiaoyu Shi[1,5,9,10,*]

**Affiliations:**
[1] Center for Complex Biological Systems, University of California, Irvine; Irvine, 92697, United States.
[2] Physiology and Biophysics, University of California, Irvine; Irvine, 92697, United States.
[3] Department of Bioengineering and Therapeutic Sciences, University of California, San Francisco; San Francisco, 94143, United States.
[4] School of Biomedical Engineering, Science and Health Systems, Drexel University; Philadelphia, PA19104
[5] Department of Developmental and Cell Biology, University of California, Irvine; Irvine, 92697, United States.
[6] Current Address: School of Criminal Justice and Criminalistics, California State University, Los Angeles; Los Angeles, 90042, United States.
[7] Cardiovascular Research Institute, School of Medicine, University of California, San Francisco; San Francisco, 94143, United States.
[8] Laboratory for Fluorescence Dynamics, University of California, Irvine; Irvine, 92697, United States.
[9] Department of Biomedical Engineering, University of California, Irvine; Irvine, 92697, United States.
[10] Department of Chemistry, University of California, Irvine; Irvine, 92697, United States.

*Corresponding author: Xiaoyu Shi. Email: xiaoyu.shi@uci.edu

**Abstract:**

Elucidating the spatial relationships within the protein interactome is pivotal to understanding the organization and regulation of protein-protein interactions. However, capturing the 3D architecture of the interactome presents a dual challenge: precise interactome labeling and super-resolution imaging. To bridge this gap, we present the Proximity Labeling Expansion Microscopy (PL-ExM). This innovation combines proximity labeling (PL) to spatially biotinylate interacting proteins with expansion microscopy (ExM) to increase imaging resolution by physically enlarging cells. PL-ExM unveils intricate details of the 3D interactome's spatial layout in cells using standard microscopes, including confocal and Airyscan. Multiplexing PL-ExM imaging was achieved by pairing the PL with immunofluorescence staining. These multicolor images directly visualize how interactome structures position specific proteins in the protein-protein interaction network. Furthermore, PL-ExM stands out as an assessment method to gauge the labeling radius and efficiency of different PL techniques. The accuracy of PL-ExM is validated by our proteomic results from PL mass spectrometry. Thus, PL-ExM is an accessible solution for 3D mapping of the interactome structure and an accurate tool to access PL quality.

**Keywords:** proximity labeling, Expansion Microscopy, super resolution, interactome

**INTRODUCTION**

Most cellular functions are realized by a set of protein-protein interactions (PPIs) called the protein interactome. Studies on the interactome of a hub protein transform our understanding of health and diseases and aid in discovering therapeutic targets[1-4]. Recent advancements in microscopy significantly advanced our understanding of protein interactomes by providing structural information from atomic to organellar scales. Cryo-electron microscopy uncovers atomic details of interacting proteins that predict binding sites. Super-resolution microscopy reveals molecular details that provide spatial relationships between specific interacting proteins. Scanning electron microscopy maps the overall proteome distribution which provides a global landscape of PPIs. Yet, visualization of the 3D architecture for the interactome has lagged[4,5].

Visualizing the structural context of PPIs is essential for understanding how PPIs are organized by protein assembly and influenced by their subcellular environment. For example, by locating the activation of extracellular-signal-regulated kinase (ERK) by G-protein-coupled receptors (GPCRs) at endosomes, Kwon et al. identified a non-canonical mechanism of spatial regulation of ERK signaling through endosomal signaling[5]. Pownall et al. used ChromExM of embryos to reveal how the pioneer factor Nanog interacts with nucleosomes and RNA polymerase II (Pol II), providing direct visualization of transcriptional elongation as string-like nanostructures. The structural information of the interactome can enable us to discover new PPI mechanisms. There is an urgent need for imaging methods that can dissect the spatial relationships in the interactome.

Capturing the 3D architecture of the interactome presents a dual challenge: precise interactome labeling and super-resolution imaging. Precise interactome labeling should highlight the interactome of a targeted protein from the whole proteome of a cell. Proximity labeling (PL) emerged as a powerful technique that spatially selects proteins within its labeling resolution from the protein of interest. In this method, the protein of interest is fused to or labeled by an enzyme. When activated, this enzyme modifies nearby proteins by attaching a small marker like biotin to them. Proximity-labeled proteins can be subsequently analyzed by mass spectrometry (PL-MS) as potential interaction partners with the protein of interest. Several proximity labeling methods, such as HRP[6-8], APEX[9-11], BioID[12-14], TurboID[15, 16], and µMap[1] have been widely used with mass spectrometry (MS) to identify the organellar proteome[10, 17] and network of interactions in cells[14, 18-20]. These PL methods paved the way for interactome visualization by precisely labeling the interactome.

The second challenge in interactome visualization is simultaneously imaging specific proteins and its interactome structure with super resolution. Although super-resolution light microscopy can specify proteins and electron microscopy can visualize proximity-labeled proteins, it is difficult to simultaneously resolve both with the matching resolution. An emerging super-resolution technique called expansion microscopy (ExM) raised a promising solution. ExM is a chemical approach to increase the resolving power of any microscope by physically expanding cells by 4-20 times in each dimension [21]. The early versions of ExM methods use antibodies and fluorescent proteins to label proteins, which

90  only allow targeted protein imaging[22-24]. Excitingly, recent advances in ExM enabled
91  super-resolution imaging of nonspecifically labeled biomolecules as the context channel
92  in addition to the immunostained specific proteins. For instance, Mao et al. and M'saad
93  et al. respectively demonstrated the power of their FLARE[25] and pan-ExM[26] methods in
94  imaging the entire protein, lipid, and carbohydrate landscape. In another study, Pownall
95  and colleagues mapped chromatin with single-nucleosome resolution using their
96  technique chromExM[27]. Klimas et al. developed a Magnify protocol that retains nucleic
97  acids, proteins and lipids in a uses a mechanically sturdy gel[28]. Beyond protein and DNA
98  landscape, Sun et al. developed click-ExM enabling imaging of all biomolecules including
99  glycans and small molecules[29]. These approaches collectively spotlight the ability to
100 delineate specific proteins within context structures at a matching super-resolution.
101 However, a glaring gap persists as ExM has not yet been used in studying the
102 interactome, underscoring an unaddressed demand in interactome visualization.

103 We report proximity labeling expansion microscopy (PL-ExM), which simultaneously
104 images the 3D architecture of the interactome and specific interactive proteins with super-
105 resolution (Figure 1A). PL-ExM uses PL to label the interactome, antibodies to specify
106 proteins of interest, and ExM for super-resolution imaging. The advantage of ExM over
107 super-resolution light microscopy, such as STORM and STED, is its fast speed, high
108 imaging depth, and low requirement for advanced microscopes. Using PL-ExM, we can
109 locate specific proteins on the 3D structure of their interactome with a resolution up to 12
110 nm on commonplace microscopes, such as confocal and Airyscan. PL-ExM is compatible
111 with any PL methods that can biotinylated proteins, for example, APEX and HRP labeling.
112 Interestingly, HRP-catalyzed tyramide signal amplification (TSA) was recently used to
113 amplify signals for ExM [30], but not for interactome visualization. PL-ExM was designed
114 and optimized for the opposite purpose, that is proteome characterization.
115

116 Beyond imaging, this method can assess the quality of PL. Despite its importance of PL,
117 the variability in the labeling resolution and efficiency of PL experiments often leads to
118 limited overlap in PL-MS results, even when analyzing the interactome of the same
119 targeted protein[31]. For example, a study showed less than 25% overlap in interactomes
120 detected by APEX2 and BioID for the same bait valosin-containing protein (VCP) [19].
121 Oakley et al. observed a 5-fold difference in labeling radius between μMap and
122 peroxidase-based PL using STED[32]. Using PL-ExM, we compared the labeling radius and
123 efficiency between APEX2 and HRP labeling, and between various labeling durations. To
124 validate the PL-ExM imaging in evaluating PL quality, we profiled the interactome using
125 PL-MS in parallel.  The agreement between our imaging and MS data confirms that PL-
126 ExM is a reliable and accurate tool for PL quality control.

127 We will unfold the workflow of PL-ExM and demonstrate its capability of interactome
128 visualization and PL assessment as follows.
129

130 **RESULTS**

131 **Principle and workflow**

132 PL-ExM provides super-resolution to dissect the 3D architecture of the interactome by
133 physically expanding the proximity-labeled cells and tissues in the swellable hydrogel.

The effective imaging resolution of an expanded sample is equal to the microscope resolution divided by the length expansion factor of the sample. PL-ExM is compatible with most light microscopes, such as confocal, Airyscan, light sheet, SIM, STORM, and STED, and most ExM protocols which result in different expansion factors. For example, if the proximity labeled sample is expanded by four times and imaged with a confocal with a resolution of 280 nm, the effective imaging resolution will be 70 nm.

The swellable hydrogel that is made of different recipes and expansion procedures can expand from 3 to 14 times. The most commonly used gel formula for expansion microscopy consists of acrylamide, sodium acrylate, ammonium persulfate (APS), N,N,N′,N′-Tetramethylethylenediamine (TEMED), and N-N′-methylenebisacrylamide [24, 33, 34]. This hydrogel expands about 4 times in pure water. By adjusting the crosslinkers or hydrolysis duration, the hydrogel can expand up to 13 times in one round [35-39]. Multiple rounds of expansion even achieve a length expansion factor of 15 to ~20x [40]. The sample expansion improves the resolving power of the microscope by a factor from 3 to 20 depending on the expansion protocol. With different combinations of the microscope and the expansion protocol, PL-ExM achieves super resolution ranging from 12 nm to 70 nm, allowing visualization of a burst of structural details in the interactome that was not resolvable by diffraction-limited microscopes alone (Figure 1A).

The workflow of PL-ExM includes 6 steps (Figure 1B): 1. PL and immunostaining, 2. adding protein anchors, 3. gelation, 4. homogenization, 5. fluorescent staining, and 6. expansion. Technically, any PL method can be used as step 1. Peroxidase-based PL of mitochondria is showcased in our workflow because it is widely used. Peroxidase HRP or APEX2 is first introduced to bait protein of the interactome. In the presence of hydrogen peroxide ($H_2O_2$) and biotin-phenol, proteins within a labeling radius of the peroxidase are biotinylated. Additionally, a protein of interest is immunostained by antibodies conjugated with digoxigenin (antibody-DIG). Following the PL and immunostaining is the expansion procedure consisting of steps 2 to 6. In Step 2, proteins are chemically modified with anchoring molecules, such as glutaraldehyde (GA), methacrylic acid N-hydroxysuccinimide ester (MA-NHS), or glycidyl methacrylate (GMA). These anchors serve the same goal: covalently crosslinking proteins to polyacrylic chains when polyacrylic hydrogel is formed inside and outside of the cells in Step 3. Next, cells that are embedded in the hydrogel are homogenized by proteinase K digestion or heat denaturation (Step 4). The homogenization breaks the protein interactions to allow isotropic sample expansion in the final expansion step (Step 6). Before expansion, the biotinylated interactome and DIG-labeled proteins of interest are stained by fluorescently conjugated streptavidin and anti-DIG antibodies, respectively (Step 5). The reason to introduce fluorescent dyes after gelation is that free radical polymerization reactions can significantly quench fluorescent dyes [23, 24, 34, 36, 41, 42]. We have demonstrated that post-gelation fluorescence staining of biotin or DIG probes can increase the signal-to-noise ratio of ExM images by several folds in our Label-Retention Expansion Microscopy (LR-ExM) technique[34]. Through the 6 steps, PL, ExM, and LR-ExM are streamlined into one workflow of PL-ExM.

Detailed chemical reactions underlining each step in the workflow are described in Figure S1.
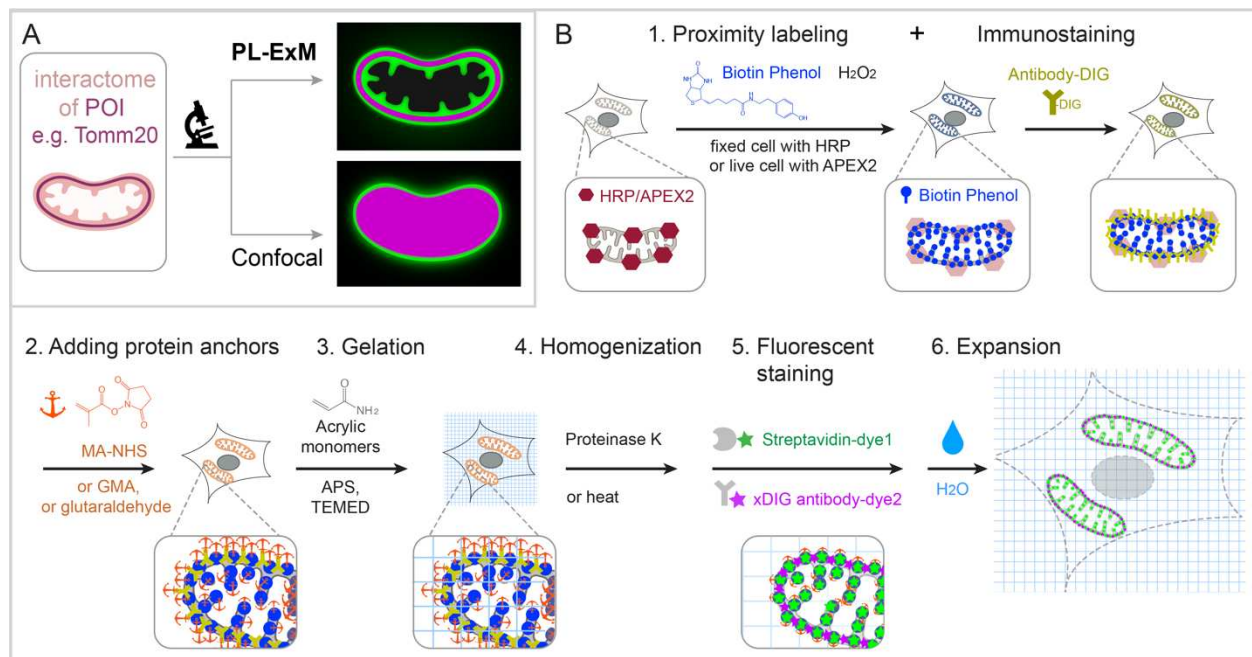
178

**Figure 1. Graphic abstract and workflow of PL-ExM.** In the showcase, Tomm20 is the bait for the PL and the target for the immunostaining. (A) Graphic abstract of PL-ExM method. PL-ExM offers super resolution to visualize small interactome structures that present the ground truth. Diffraction-limited microscopy, such as confocal microscopy, misses structural details in the ground truth. (B) The PL-ExM workflow comprises six steps. 1. Proximity labeling catalyzed by enzymes (HRP, APEX, etc.) and delivered by biotin phenol. Following PL, a protein of interest is labeled with antibodies conjugated with DIG. 2. Adding protein anchors, such as MA-NHS, GMA or glutaraldehyde. 3. Gelation with acrylic and acrylate monomers. 4. Denaturation using proteinase K or heat denaturation. 5. Fluorescent staining: stain the biotin and DIG with fluorescently conjugated streptavidin and anti-DIG antibodies. 6. Expansion: expand hydrogel through immersion in pure water.

190

## PL-ExM provides super resolution to visualize the 3D interactome architecture

We demonstrated the resolution improvement of PL-ExM by comparing the images of proximity-labeled mitochondria with and without expansion (Figure 2). The bait protein is the outer mitochondrial membrane (OMM) protein TOMM20, which was immunostained with antibodies conjugated with HRP. Proteins within the labeling radius of HRP were biotinylated by biotin-phenol in the presence of hydrogen peroxide. The PL duration was 30 seconds. The TOMM20 was also immunostained with antibody-DIG as the second color channel. Both expanded and non-expanded samples were imaged with the same Airyscan microscope, which has a measured resolution of 180 nm (Figure S2). Since this resolution was much larger than the labeling radius of HRP, images of non-expanded samples failed to encapsulate the intricate details of the mitochondria (Figure 2 A, B-E). On the contrary, PL-ExM imaging of 4.2 times expanded samples resolved the hollow structure of mitochondria (Figures 2J) and sometimes the mitochondria cristae (Figures S3B&S4B) with its 43 nm effective resolution. This observation of the hollow structure with high signal at the periphery and a medium signal inside (Figure 2J) indicated that the

206    HRP proximity labeling of TOMM20 not only biotinylated proteins on the outer
207    mitochondrial membrane, such as translocases of the outer membrane (TOMs), but also
208    the ones inside, such as translocases of the inner membrane (TIMs). The protein
209    identities are confirmed in our PL-MS analyses (Figure 4P).

210    The resolution of PL-ExM can be further improved with larger expansion factor. We
211    expanded proximity-labeled cells by 8.2 times using the TREx protocol [38]. As a result, x8
212    PL-ExM provided 22 nm resolution, which resolved two narrow and well-separated peaks
213    of proximity-labeled proteins at the cross-section of mitochondrion (Figures 2P&R). The
214    distance between the two peaks showed that the mitochondrion had a diameter of 500
215    nm (Figure 2R). The full width of the half maximum (FWHM) of each peak represented a
216    PL resolution of 0.37µm (Figure 2R). In summary, PL-ExM can significantly increase the
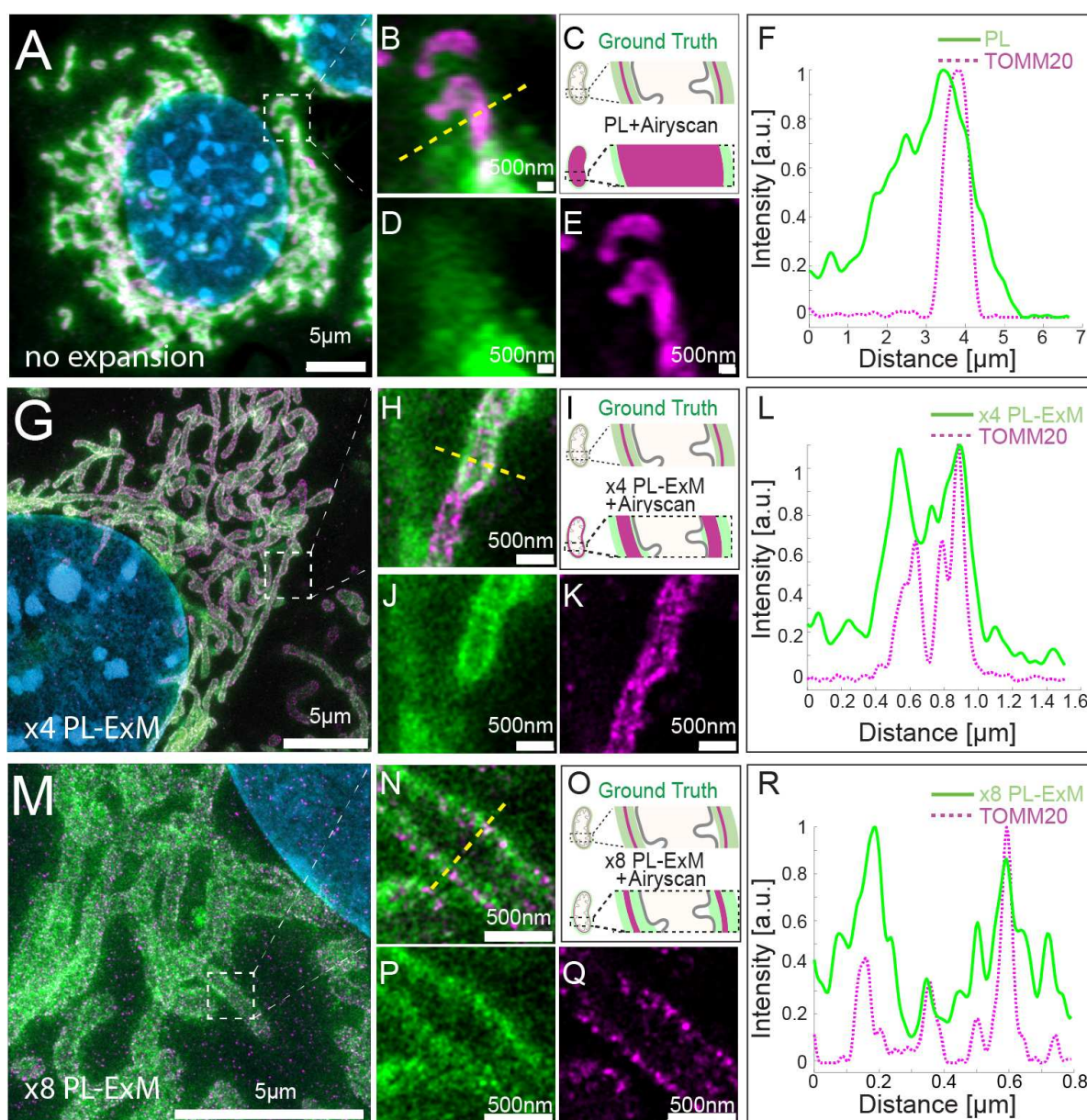217    effective imaging resolution by 4 to 8 times with a single round of expansion.



218

219 **Figure2. PL-ExM offers super resolution for the visualization of the proximity-labeled**
220 **interactome landscape.** All images were taken on MEF cells labeled with two colors in the same
221 way. The TOMM20 was proximity-labeled to show its interactome (green) and simultaneously
222 immunostained to locate the protein of interest (magenta). The nucleus was stained with DAPI
223 (blue). All images were taken with Airyscan microscope. (A) Representative image of a non-
224 expanded sample. (B) Magnified view of the boxed region in (A). (C) Schematics of the ground
225 truth structure of proximity-labeled TOMM20 (green) and immunostained TOMM20 (magenta),
226 and the expected image without expansion. (D) PL channel of (B). (E) Immunostained TOMM20
227 channel of (B). (F) A representative histogram showing the fluorescence intensity in a cross
228 section of a mitochondrion from the image (B) of the non-expanded sample. The fluorescence
229 intensity was denoised and normalized with respect to each channel. (G) Representative PL-ExM
230 image of a 4-time expanded sample, named x4 PL-ExM. (H) Magnified view of the boxed region
231 in (G). (I) Schematics of the same ground truth as in (C), and the expected PL-ExM image of the
232 4-time expanded sample. (J) PL-ExM channel of (H). (K) Immunostained TOMM20 channel of
233 (H). (L) A representative histogram showing the fluorescence intensity in a cross section of
234 mitochondrion from a x4 PL-ExM image. (M) Representative PL-ExM image of an 8-time
235 expanded sample, named x8 PL-ExM.  (N) Magnified view of the boxed region in (M). (O)
236 Schematics of the same ground truth as in (C), and the expected PL-ExM image of the 8-time
237 expanded sample. (P) PL-ExM channel of (N). (Q) Immunostained TOMM20 channel of (N). (R)
238 A representative histogram showing the fluorescence intensity in a cross section of mitochondrion
239 from an x8 PL-ExM image. In all histograms (F,L&R), the fluorescence intensity was denoised
240 and normalized with respect to each channel. (A, G, M, N, P, Q) are maximum intensity projections
241 of z stacks. (B, D, E, H, J, K) are single-slice images of 3D z stacks. Length expansion factors are
242 4.2 for samples (G, H, J, K), and 8.2 for (M, N, P, Q).  All scale bars are in pre-expansion units.
243

## Multiplex Imaging reveals spatial relationships between interactive proteins.

245 In the previous section, we used two-color PL-ExM to visualize the spatial relationship
246 between the bait protein TOMM20 in its mitochondrial interactome. In this section, we
247 demonstrated how to identify other interactive proteins in the interactome using the same
248 method, with the following two examples.

249 Previous studies suggested that clathrin-coated pits (CCPs) are transported on
250 microtubules based on live cell imaging [43, 44]. Here, we try to confirm the CCP-microtubule
251 interactions by directly locating CCPs in the microtubule interactome. We imaged
252 immunostained Clathrin A (CLTA) and proximity-labeled $\alpha$-TUBULIN using two-color PL-
253 ExM (Figures 3A-G). Thanks to the super resolution, the images show that the proximity-
254 labeled proteins not only displayed the microtubules but also showed clusters budding
255 from the microtubules (pointed by arrows in Figures 3C&F). Interestingly, many of these
256 clusters were found to be partially overlapping with the immunostained CCPs (Figures
257 3B&E). This is a direct visualization of CCPs as components of the interactome of
258 microtubules, which affirms that CCPs interact with microtubules. Such spatial
259 relationships in interactomes were not detectable without expansion due to limited
260 resolution (Figures 3H-N).

261 We further applied PL-ExM on the primary cilium, a more challenging organelle with less
262 abundant and tiny size (Figures 3O-R). The primary cilium is a sensory organelle that
263 organizes signaling pathways, such as sonic hedgehog signaling, and their regulatory

264     GTPases, such as ADP-ribosylation factor-like protein 13B (ARL13B). Mick et al.
265     developed a groundbreaking method called cilia-APEX, which proximity-labeled ciliary
266     interactome or MS analysis[45]. Using this method, they identified new components of
267     cargos transporting GPCRs in cilia. Here, our aim is to use PL-ExM as a complementary
268     method to cilia-APEX proteomics, providing spatial information. In this demonstration, we
269     investigated a specific question: do the distal appendages (DAs) located at the base of
270     the cilium mediate ARL13B entry or exit from the primary cilium? We simultaneously
271     imaged proximity-labeled DA component CEP164 and immunostained ARL13B in MEF
272     cells, using the two-color PL-ExM.  With an 8.4-time expansion, we were able to resolve
273     the donut-shaped DA disk and the distribution of AL13B through the cilia (Figure 3P).  The
274     images showed negligible overlapping between the interactome of CEP164 and ARL13B
275     (Figures 3Q&R). The results indicated that the ARL13B either has no interaction or has
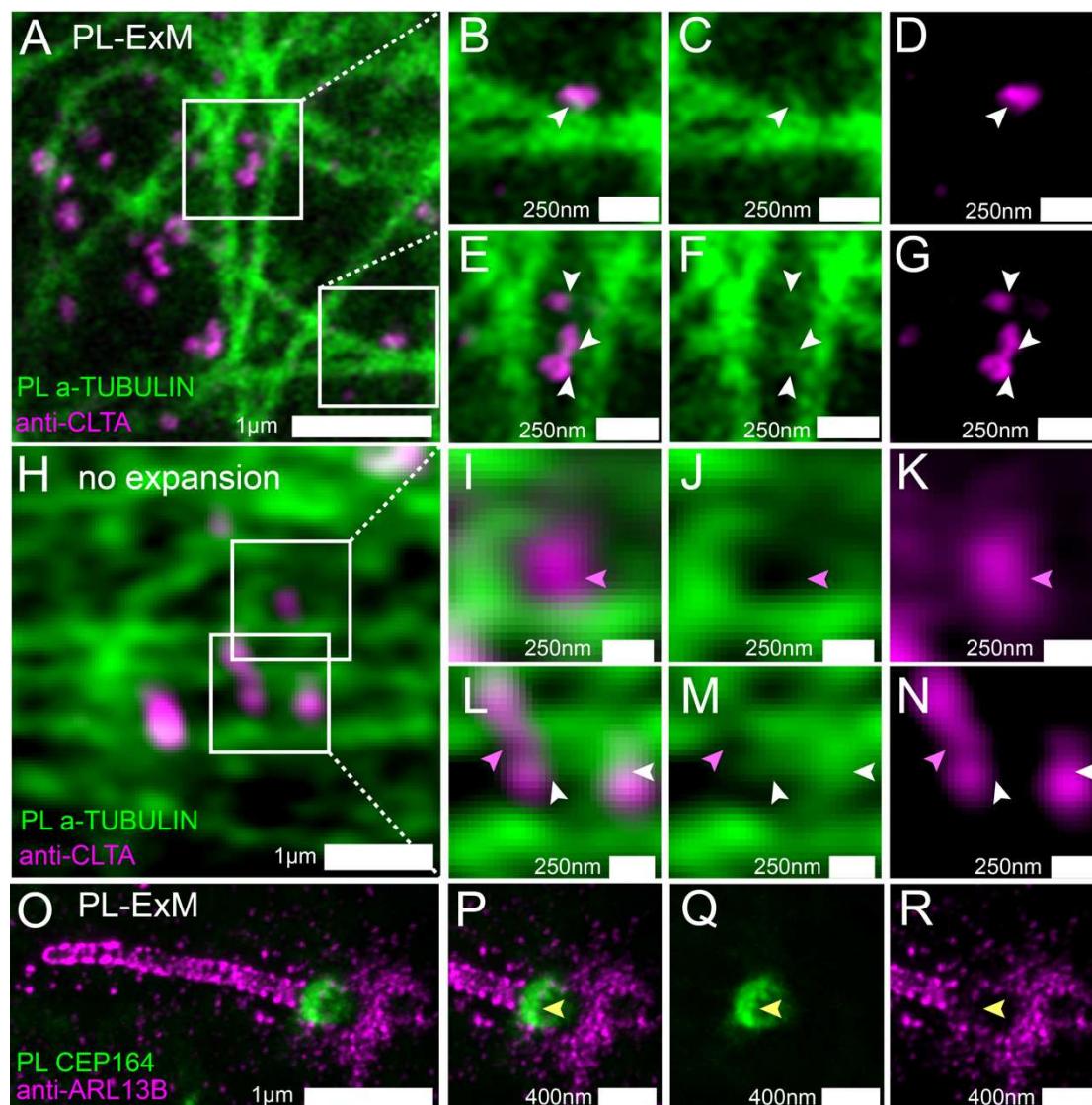276     very transient interaction with DAs.



277

278     **Figure 3. Two-color PL-ExM images dissect spatial relationships between interactive**
279     **proteins.** (A-G) PL-ExM images of proximity-labeled α-TUBULIN (green) and immunostained

280 CLTA (magenta) in U2OS cells. (B-G) Magnified view of the boxed regions in (A). The white arrows
281 indicate the co-localization of CCPs and bud-like structures stemming from microtubules. (H-N)
282 Airyscan images of proximity-labeled $\alpha$-TUBULIN (green) and immunostained CLTA (magenta) in
283 U2OS cells without expansion. (I-N) Magnified view of the boxed regions in (H). The pink arrows
284 point at CCPs that do not co-localize with microtubules. White arrows indicate possible
285 colocalization of CCPs and microtubule structures. (O-R) PL-ExM of proximity-labeled CEP 164
286 (green) and immunostained ARL13B (magenta) in a primary cilium of a MEF cell. (P-R) Magnified
287 view of the ciliary base in (O). The yellow arrows indicate anti-localization between ARL 13B and
288 CEP 164. (A-N) are single-slice images. (O-R) are maximum intensity projections of z stacks. The
289 length expansion factors are 4.1 (A-G) and 8.4 (O-R). All images are taken by an Airyscan
290 microscope. All scale bars are in pre-expansion units.
291

292 **PL-ExM assesses the resolution and efficiency of proximity labeling.**

293 Despite PL's capability of labeling interactomes, the labeling resolution and efficiency vary
294 in each experiment. The parameters that cause the variability include the choice of
295 enzyme, such as HRP and APEX2, the choice of labeling probes, such as different
296 phenols, as well as the labeling duration[1, 46]. In this section, we will demonstrate how PL-
297 ExM assesses PL under different enzymes (APEX2 vs HRP) and durations (30 seconds
298 vs 20 minutes). We evaluated the quality of PL in each condition based on two important
299 characteristics: labeling resolution and efficiency. The labeling resolution determines the
300 spatial selectivity of the interactome and positive false rates, while the labeling efficiency
301 indicates the coverage of the interactome.  We used the average mitochondrial diameter
302 (n$\geq$90) measured from PL-ExM images as the readout of labeling resolution and total
303 fluorescence intensity to compare the labeling efficiency between PL conditions. For fair
304 comparison, all samples to be compared were labeled in the same batches (n>3) and
305 imaged under the same microscope settings on the same days.

306 We compared two commonly used enzymes, APEX2 and HRP using PL-ExM.
307 Mitochondrial outer membrane proteins were chosen as the bait proteins because their
308 interactomes were extensively studied with PL-MS[10, 47]. The proteomic data can be used
309 as references to validate our PL-ExM assessment. APEX2-catalyzed PL was performed
310 on U2OS cells overexpressing *APEX2-OMM* (Figure 4A), where OMM is a peptide on the
311 outer mitochondrial membrane. HRP-catalyzed PL was performed on U2OS cells which
312 had TOMM20 immunostained with HRP-conjugated antibodies (Figure 4C). The same
313 biotin-phenol and reaction duration were given in HRP and APEX2-cataluyzed PL. PL-
314 ExM showed that the HRP-catalyzed PL achieved about four times higher labeling
315 efficiency than the APEX2 condition (Figures 4B,D&E). In addition, The PL catalyzed by
316 HRP also exhibited higher labeling resolution than APEX2, showing a smaller
317 mitochondrial diameter of 0.56μm ± 0.030μm. (Figure 4G). On contrary, APEX2-catalyzed
318 PL showed more diffusive signal around mitochondria (Figure 4A), resulting in a bigger
319 mitochondrial diameter of 0.97μm ± 0.065μm (Figure 4F). The lower labeling efficiency
320 and lower labeling resolution of APEX may be attributed to the limited permeability of
321 biotin-phenol in live cells and the lower catalytic activity of APEX compared with HRP.

322 We also evaluated the PL quality with two labeling durations: 30 seconds and 20 minutes
323 (Figures 4H-N). HRP was used to proximity label the TOMM20 in both conditions. The

324 only difference is the duration of $H_2O_2$ treatment. We observed a nearly quadrupled
325 labeling efficiency in the 20-minute condition, compared with the 30-second condition
326 (Figure 4L). However, the diameter of the mitochondria measured from the two conditions
327 did not differ that much. PL-ExM images of the 20-minute group showed a considerably
328 larger mitochondrial diameter (0.79μm, Figure 4M), compared with 0.56μm of the 30-
329 second group (Figure 4N). These results indicate the labeling efficiency of HRP-catalyzed
330 PL significantly increases over time, while the labeling resolution drops only slightly. This
331 finding underscores the importance of the PL treatment duration as a crucial variable that
332 requires meticulous calibration based on the research objective.

333 To assess PL-ExM accuracy, we compared PL-MS and PL-ExM results from identically
334 prepared samples as described above. The cells biotinylated by APEX2 and HRP were
335 lysed, affinity purified, digested, and analyzed by MS. In comparison to non-labeled
336 controls, label-free based quantitative MS analyses revealed that both APEX2 and HRP
337 methods were able to enrich mitochondrial proteins (Figures 4O&P), which are
338 comparable to a previous report using APEX2-IMS (Figure 4P) [10]. Interestingly, HRP
339 samples yielded stronger labeling of TIMs and TOMs proteins than the APEX2 samples,
340 suggesting HRP-catalyzed PL was less diffusive and more effective in labeling proteins
341 in closer proximity to the bait (TOMM20) (Figure 4Q). This observation is in good
342 agreement with PL-ExM images. In summary, PL-ExM emerges as an invaluable tool in
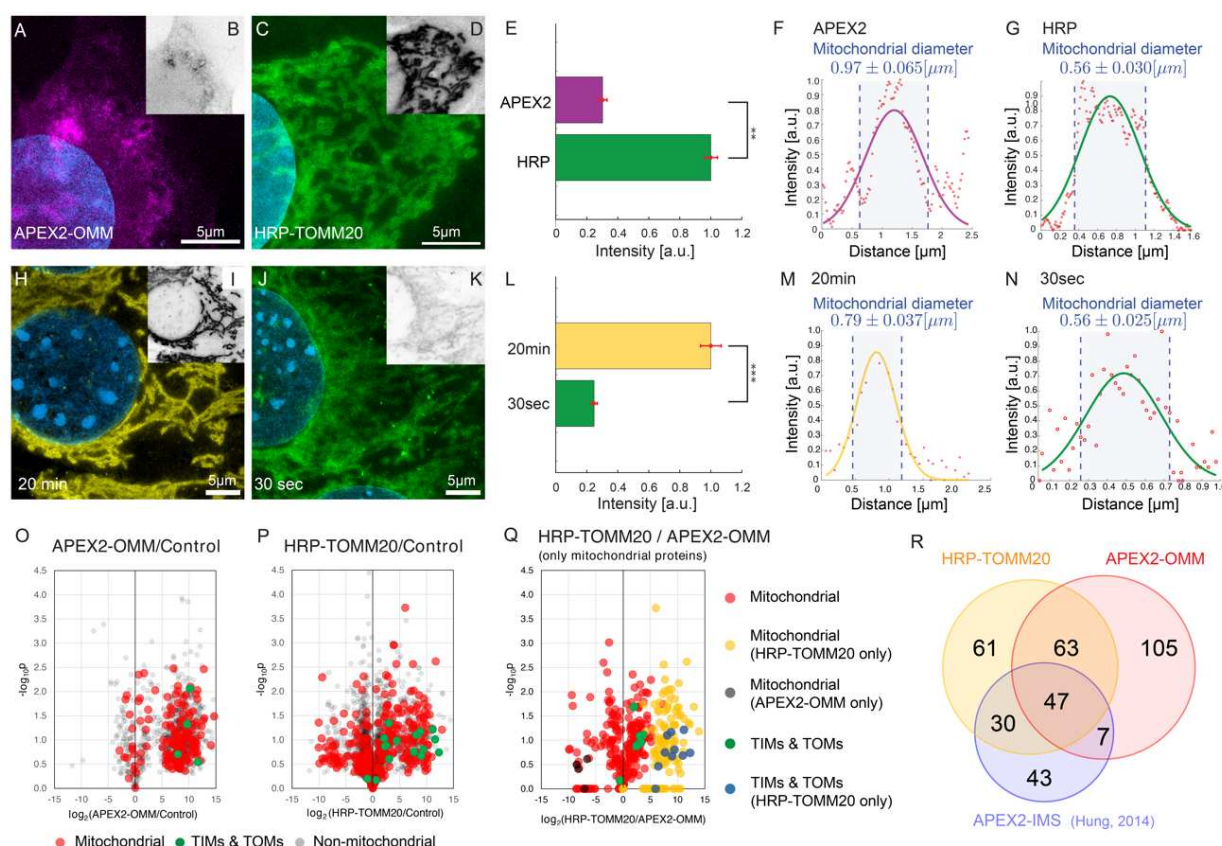343 ascertaining the optimal experimental conditions for PL.



344

**Figure 4. PL-ExM evaluates the labeling resolution and efficiency of APEX2- and HRP-catalyzed PL.** In the comparison between APEX2 and HRP (A-N and O-R), APEX2-catalyzed PL was performed on U2OS cells overexpressing *APEX2-OMM*. HRP-catalyzed PL was performed on U2OS cells which had TOMM20 immunostained with HRP-conjugated antibodies. All images were taken on a confocal microscope with the same imaging condition. (A) Representative PL-ExM image of APEX2-catalyzed PL. (C) Representative PL-ExM image of HRP-catalyzed PL. (B,D) Grayscale images of A and C respectively. Brightness and contrast are set the same for these two images for the quantitative comparison. (A-D) are maximum intensity projections of 3D z-stacks for the same z depth. (E) The bar chart summarizes the fluorescence intensity of PL-ExM images of APEX2 and HRP samples. n ≥3 per condition. The reported p-value is smaller than 0.01. (F) A representative histogram showing the fluorescence intensity in a cross-section of a mitochondrion from a PL-ExM image of an APEX2 sample. The measured mitochondrial diameter is 0.97 ± 0.065µm. The mean and a standard error were obtained from 90 measurements across 3 independent samples. (G) A representative histogram showing the fluorescence intensity in a cross-section of a mitochondrion from a PL-ExM image of a HPR sample. The measured mitochondrial diameter is 0.56 ± 0.030µm. The mean and standard error were obtained from 90 measurements across 3 independent samples. In the comparison between 20-minute and 30-second reaction duration (H-N) HRP-catalyzed PL was performed on MEF cells that had TOMM20 immunostained with HRP-conjugated antibodies. (H) Representative PL-ExM image of HRP-catalyzed PL with 20-minute $H_2O_2$ treatment. (J) Representative PL-ExM image of HRP-catalyzed PL with 30-second $H_2O_2$ treatment. (I, K) Grayscale images of H, J respectively. Image brightness and contrast are set to be the same for the quantitative comparison. (A-K) Images are maximum intensity projections of 3D z stacks for the same z depth. (L) Labeling efficiency comparison between samples with 20-minute and 30-second $H_2O_2$ treatment. 20-minute samples show ~4 times higher labeling efficiency than 30-second samples with p-value smaller than 0.001. The bar chart summarizes the fluorescence intensity of PL-ExM images from 20-minute and 30-second samples. n ≥3 per condition. (M) A representative histogram showing the fluorescence intensity in a cross-section of a mitochondrion from a PL-ExM image of a 20-minute sample. The measured mitochondrial diameter is 0.79 ± 0.037 µm. The mean and standard error were obtained from 90 measurements across 3 independent samples. (N) A representative histogram of a 30-second sample. The measured mitochondrial diameter is 0.56 ± 0.025 µm. The mean and standard error were obtained from 90 measurements across 3 independent samples. (O-P) Volcano plots depicting protein enrichment by APEX2-OMM (O) and HRP-TOMM20 (P). Fold-change is represented in log2 along x-axis, calculated as the relative normalized abundances of proteins in labeled/control. Subunits of the TIM/TOM complex are shown in green, while other mitochondrial proteins defined by MitoCarta are shown in red. Non-mitochondrial proteins are shown in gray. (Q) Mitochondrial protein enrichment by APEX2-OMM versus HRP-TOMM20. Log2 fold-change is represented along x-axis, calculated as the relative normalized abundances of proteins from HRP-TOMM20/APEX2-OMM. TIM/TOM complex subunits quantified by both APEX and HRP labeling shown in green, while those only quantified by HRP are shown in blue. The remaining mitochondrial proteins are shown in red, unless only quantified by APEX (black) or HRP labeling (blue). (R) Overlaps of enriched mitochondria proteins by APEX2-OMM, TOMM20-HRP, and APEX2-IMS[10]. The length expansion factors of PL-ExM images (A, C, H, J) are 4.1 ~ 4.2. All scale bars are in pre-expansion units, and they are 5µm.

**PL-ExM is compatible with tissues.**

In previous sections, we have demonstrated the compatibility of different PL-ExM cell lines, such as U2OS and MEF used in Figures 1-4. Here, we move forward to apply PL-ExM to tissues. Since live cell PL is usually not applicable to tissues, we recommend the

394  HRP-catalyzed PL approach of PL-ExM for interactome visualization for tissues. This way,
395  HRP is tagged to the protein of interest in fixed tissue samples by antibodies. As a
396  showcase, we applied HRP PL-ExM to mouse brains expressing neuron-specific marker
397  Thy1 with YFP. We proximity-labeled Thy1 in the brain sections using the HRP approach
398  (see Methods for more details). The x4 PL-ExM images displayed the distribution of the
399  proximity-labeled interactome of protein Thy1 across the brain section (Figure 5A).
400  Compared with cultured cells, the noise level of PL of tissues was higher. However,
401  individual dendrites and axons of neurons can be clearly seen in the PL channel (green
402  in Figure 5B). Furthermore, we co-immunostained an astrocyte marker Glial fibrillary
403  acidic protein (GFAP) in the brain tissue. The two-color images showed the spatial
404  entanglement between astrocytes and neurons, indicating their interactions (Figure 5B).

405  Deep imaging of tissue samples poses inherent challenges owing to the light scattering
406  between layers of cell and extracellular matrix. The expansion procedure of PL-ExM
407  transforms the intact tissue into a hydrogel that is optically transparent, sharing the same
408  clearing principle with CLARITY [48]. Therefore, PL-ExM offers tissue clearing for more
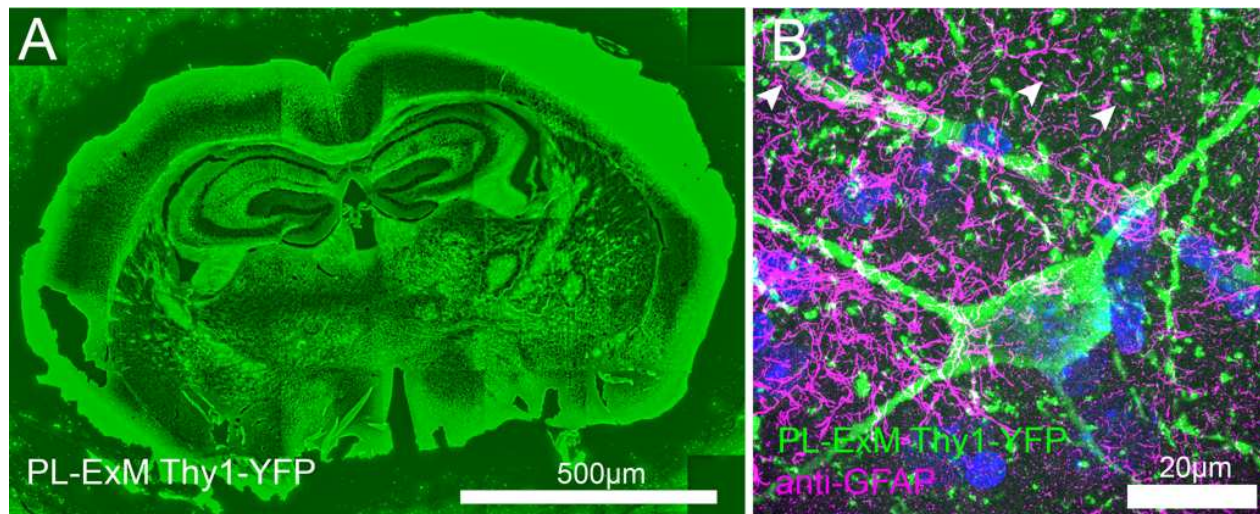409  clear and deeper visualization of the tissue structure, in addition to the super resolution.

410



411  **Figure 5. Two-color PL-ExM imaging reveals interactions in mouse brain tissues.** Both
412  images are Airyscan PL-ExM images of 20-µm sections of a mouse brain expressing Thy1-YFP
413  with proximity-labeled Thy1-YFP (green) and immunostained GFAP (magenta). (A) Proximity-
414  labeled Thy1-YFP channel of a whole mouse brain slice with. (B) A magnified view of (A) with
415  both proximity labeled Thy1-YFP (green) and immunostained GFAP (magenta). Both mages are
416  maximum intensity projections of z stack. The scale bars are 500 µm for (A) and 20µm for (B).
417  The length expansion factor is 4.0. All scale bars are in pre-expansion units.
418

419  **DISCUSSION**

420  During the expansion procedure of PL-ExM, the homogenization step breaks down
421  protein-protein interactions and the hydrogel expansion pulls interacted proteins away.
422  There might be a question: will the breakdown of protein-protein interactions cause
423  incomplete interactome detection in the images? The answer is no. It is because the
424  interactome is defined by the PL, not the expansion. Proteins within the labeling radius

425     are marked by biotin during the PL reaction when the cells are intact before the expansion
426     procedure. Therefore, as long as the biotin signal can be detected after expansion, the
427     breakdown of protein-protein interactions during the expansion procedure will not cause
428     incomplete interactome detection. The highly efficient detection of biotin after expansion
429     was proved by LR-ExM method that we recently developed [34].

430     The next question is about the fidelity of expansion. If the expansion is anisotropic,
431     distortion of the interactome structure could happen during the expansion step, resulting
432     in unreliable observation. Our team, along with other ExM developers, have rigorously
433     ensured isotropic expansion, with optimization of fixation methods, protein anchoring
434     efficiency, sample homogenization, and hydrogel recipes [22, 42, 49, 50]. We have
435     comprehensively discussed the solutions to make isotropic expansion of different
436     biological samples in a recent review [42]. This PL-ExM method is optimized for faithful
437     expansion of proximity-labeled samples with different enzymes and reaction conditions.
438     Either MA-NHS, glutaraldehyde, or glycidyl methacrylate worked well for the anchoring of
439     biotinylated proteins. Like other ExM protocols, proteinase K digestion is a reliable sample
440     homogenization method in PL-ExM. In quantitative comparison of different PL methods,
441     it is important to apply the same anchoring and homogenization reagents and conditions
442     to each sample.

443     In this work, we demonstrated 22 nm resolution by expanding cells 8.2 times using the
444     TREx protocol [38] and imaging on an Airyscan microscope (Figures 2M-R). Higher
445     resolution of PL-ExM can be achieved with up to 20 times expansion[35-40] and a more
446     advanced microscope, such as PALM, STORM, and STED. However, there is an upper
447     limit to how high the resolution can be achieved using PL-ExM. Technically, the ultimate
448     resolution is constrained by the pore size of the hydrogel before expansion. Because the
449     pore size determines how fine the hydrogel can faithfully anchor the biomolecules in their
450     initial positions. Any structural details smaller than the pore size are distorted.

451     During the method development, we found that the variabilities of PL labeling quality was
452     often overlooked. The super-resolution of PL-ExM allowed us to directly observe the
453     variation. The PL quality not only varied between methods, but also was influenced by
454     the condition of the samples and human errors. The high concentration of radical
455     quenchers in the cytosol and mitochondrial matrix[51], along with macromolecular
456     crowding[52], could impact the spatial resolution and efficiency of PL[1]. It is important to note
457     that biological systems are inherently variable and dynamic, influenced by genetics,
458     environmental conditions, or the physiological state of the sample, which can introduce
459     variability into the outcomes of PL. Therefore, we strongly recommend the developers of
460     PL methods use super-resolution imaging, such as PL-ExM, to characterize the new
461     methods. Similarly, we recommend PL-MS users to assess their sample preparation with
462     PL-ExM. The spatial information provided by PL-ExM will aid in interpreting proteomic
463     results and ruling out false positives.

464

465     **CONCLUSIONS and FUTURE DIRECTIONS**

466

467 PL-ExM significantly advances interactome imaging by uncovering the intricate spatial
468 organization of proteins within the interactome structure. By integrating the spatial
469 biotinylation of interactive proteins throughout the PL with the enhanced imaging
470 resolution offered by ExM, this method provides up to 12 nm resolution using conventional
471 microscopes, including confocal and Airyscan. Our study showcased the potential of two-
472 color PL-ExM by imaging the interactome in mitochondria, microtubules, clathrin-coated
473 pits, and primary cilia. The results revealed detailed spatial organization of specific
474 proteins within the context of the interactome architecture. The PL-ExM, which provides
475 3D structural information of the interactome, can be used as a complementary tool to the
476 PL-MS interactome analysis. As we look to the future, the next frontier for PL-ExM would
477 be to expand its multiplexity beyond the current two-color limitation. By incorporating
478 highly multiplexed immunostaining techniques, like Immuno-SABER[53], PL-ExM holds the
479 promise of mapping every individual protein within the interactome. Ultimately, the true
480 power of PL-ExM lies in its potential to unearth previously undiscovered 3D spatial
481 relationships between interactive proteins, paving the way for a deeper understanding of
482 intricate biological and pathological processes.

483 PL-ExM also stands out as a pivotal tool for gauging both the labeling resolution and
484 efficiency of PL Methods. Our evaluation of APEX2- and HRP-catalyzed PL methods
485 showed that PL-ExM has the resolving power to measure the labeling radius and has the
486 sensitivity to compare the labeling efficiency across different PL methods. PL-ExM is
487 compatible with a broad spectrum of PL methods that biotinylate proteins, including but
488 not limited to APEX, HRP, BioID, TurboID, and µMap. The congruence between our
489 imaging findings and the proteomic outcomes from PL-MS confirmed PL-ExM as a
490 reliable quality control method for PL methodologies.

## METHODS

### Cell line generation

*APEX2-OMM* gene fragment (from a plasmid Addgene #238450) was cloned into a second generation 5' self-inactivating lentiviral backbone (pHR) downstream of a SFFV promoter, using InFusion cloning (Takara Bio #638910). A pantropic VSV-G pseudotyped lentivirus was produced via transfection of Lenti-X 293T cells with the pHR transgene expression vector and viral packaging plasmids pCMVdR8.91 and pMD2.G using Fugene HD (Promega #E2312). At 48 hours, the viral supernatant was harvested, filtered through a 0.45 $\mu$m filter (Millipore #HAWP04700), and added onto the U2OS cells for transduction. *APEX2-OMM* cell lines are generated from Single-cell cloning of the transduced U2OS cells.

### Cell culture

MEF cells were cultured in DMEM, Glutamax (Thermofisher; 10566-016) supplemented with 15% Fetal Bovine Serum (FBS) and 1% antibiotics antimycotic solution (Sigma Aldrich; A5955) at 37°C in 5% CO2. U2OS (ATCC; HTB-96) and U2OS-*APEX2-OMM* cells were cultured in McCoy's 5a (ATCC; 30–2007) supplemented with 10% FBS and 1% antibiotics antimycotic solution at 37°C in 5% $CO_2$. For PL-ExM, cells were seeded at $10^4$ cells/cm$^2$ in 16-well chambers (Grace Bio-Labs; 112358) and grown to 80% confluency. For MEF cells, we coat the chamber with gelatin solution (Sigma-Aldrich; G1393-100ML) for 1 hour at 37°C. In Figure 4O-R, MEF cells were seeded at a density of $10^4$cells/cm$^2$ in 16-well chambers. After 16 hours of incubation, cells were starved for 24 hours in Opti-Mem reduced serum medium for ciliation.

### Animal Sacrifice and brain slice preparation

Thy1-YFP mice were euthanized via $CO_2$ inhalation and transcardially perfused with ice-cold 1X PBS buffer. Brains were removed carefully and fixed in freshly made 4% paraformaldehyde solution for 24 hours at 4°C. Brains were then cryoprotected in 30% sucrose solution at 4°C before embedding in OCT and storage at -80°C. Frozen brains were sectioned at 20 μm on a Leica SM2000 R sliding microtome for subsequent immunohistochemical analyses. All animal protocols were approved by the Institutional Animal Care and Use Committee (IACUC) of the University of California, Irvine.

### HRP antibody catalyzed PL for cultured cells

Fixation, endogenous peroxidase blocking, permeabilization, and endogenous biotin blocking. In figure 2, MEF cells were fixed with 3% paraformaldehyde (PFA) and 0.1% Glutaraldehyde (GA) solution for 15 minutes at room temperature, followed by reduction using 0.1% sodium borohydride in PBS for 5 minutes. In Figure 4 A-N, cells were fixed with 3.2% PFA in PEM buffer (100 mM Pipes, 1 mM EGTA, and 1 mM MgCl2, pH 6.9) at room temperature for 10 minutes, followed by reduction using 0.1% sodium borohydride in PBS for 5 minutes. In figure 4O-R, cells were fixed with 4% PFA for 15 minutes at room temperature.

530  After fixation, cells were washed with PBS for 3 times, with 5 minute interval between
531  washes. Then, cells were incubated with 3% hydrogen peroxide ($H_2O_2$, Sigma Aldrich;
532  H1009) for 5 minutes at room temperature to block the endogenous peroxidase before
533  introducing any HRP in the system. Reaction was quenched by adding 2mM of L-Ascorbic
534  acid sodium (Alfa Aesar; A17759) for 5 minutes followed by three PBS wash. The fixed
535  cells were incubated in a permeabilization/blocking buffer (3% BSA, and 0.1% Triton X-
536  100 in PBS) for 30 minutes at room temperature prior to immunostaining steps.

537  Primary antibodies at a concentration of 2 µg/ml were added to the fixed cells in the
538  blocking buffer (3% BSA in PBS) for 16 hours at 4°C. The primary antibodies used for this
539  paper are Rabbit x TOMM20 (1:250 dilution, santa cruz; sc-11415), Rat x α-TUBULIN,
540  tyrosinated, clone YL1/2 (Millipore Sigma; MAB1864-I), Rabbit x anti-clathrin heavy-chain
541  (1:100 dilution, Abcam; ab21679), Rabbit x ARL 13B (1:100 dilution, Proteintech; 17711-
542  1-AP ), Mouse x CEP164 (1:100 dilution, Santa Cruz; sc-515403), Chicken x GFAP
543  (1:1000 dilution, AbCam; ab4674),  Rabbit x GFP (D5.1,1:200, Cell Signaling; 2956). After
544  primary antibody incubation, the cells were washed with a blocking buffer for three times
545  followed by 5 minutes of incubation between washes. After washing, cells were incubated
546  with 3 µg/mL AffiniPure Goat x Rabbit (1:100, Jackson ImmunoResearch; 111-005-144),
547  Goat x Mouse (1:100, Jackson ImmunoResearch; 115-005-146), or Goat x Rat (1:100,
548  Jackson ImmunoResearch; 112-005-167) secondary antibodies in blocking buffer for
549  1hour at room temperature, then the cells were washed with a blocking buffer for three
550  times followed by 5 minutes of incubation between washes. After secondary antibody
551  staining and washing, cells were incubated with ImmPRESS HRP Horse x Goat (no
552  dilution, Vector Laboratories; MP-7405) for 1 hour followed by three washing with PBS.

553  Cells were incubated with 0.5mM biotin phenol solution (Biotin tyramide, Sigma Aldrich;
554  SML-2135) for 15 minutes at room temperature. A fresh 2mM $H_2O_2$ solution (in PBS) was
555  prepared right before the reaction, and the same volume of $H_2O_2$ solution was added to
556  the cells in the biotin phenol solution for 30 seconds if specified otherwise. After treatment,
557  the reaction was quenched with 2mM of L-Ascorbic acid sodium solution for 5 minutes at
558  room temperature.

559  **APEX2-catalyzed PL for cultured cells**

560  Permeability of biotin phenol has significant implications on the efficacy of proximity
561  labeling, emphasizing the need for careful calibration when proximity labeling is done
562  when cells are live. We tested 1mM biotin phenol incubation for 2 hours at 37°C gives the
563  best labeling results. A fresh 2mM $H_2O_2$ solution (in PBS) was prepared right before the
564  reaction, and the same volume of $H_2O_2$ solution was added to the cells in the biotin phenol
565  solution for 1 minute. After treatment, the reaction was quenched with 2mM of L-Ascorbic
566  acid sodium solution for 5 minutes, followed by three PBS washes. After proximity
567  labeling, U2OS-*APEX2-OMM* cells were fixed with 4% PFA for 15 minutes at room
568  temperature and washed with PBS for 3 times.

569  **HRP antibody catalyzed PL for mouse brain tissues**

570  We first dried a tissue slide for 30 minutes and rehydrated it for 10 minutes by immersing
571  the sample in PBS. After additionally washing the sample with PBS for 2 times, we

572    incubated a tissue sample with 3% hydrogen peroxide for 5 minutes. The reaction was
573    quenched by adding 2mM of L-Ascorbic acid sodium and incubating for 5 minutes
574    followed by PBS wash for three times. Then the tissue sample was incubated in a
575    permeabilization/blocking buffer (3% BSA, and 0.1% Triton X-100 in PBS) for an hour.
576    We performed overnight primary antibody staining at 4°C using Rabbit x GFP
577    (D5.1,1:200, Cell Signaling; 2956), followed by 2.5 hour of Goat x Rabbit secondary
578    antibody staining (1:100, Jackson ImmunoResearch; 111-005-144), and 2.5 hour of
579    tertiary staining using ImmPRESS HRP Horse x Goat (no dilution, Vector Laboratories;
580    MP-7405). After series of antibody staining, we incubated tissue sample in 0.5mM biotin
581    phenol solution (Biotin tyramide, Sigma Aldrich; SML-2135) for 15 minutes. A fresh 2mM
582    $H_2O_2$ solution (in PBS) was prepared right before the reaction, and the same volume of
583    $H_2O_2$ solution was added to tissue sample in the biotin phenol solution for 30 seconds for
584    proximity labeling. After treatment, the reaction was quenched with 2mM of L-Ascorbic
585    acid sodium solution for 5 minutes. After proximity labeling step, we performed additional
586    immunostaining on GFAP for 2.5 hours using primary antibody Chicken x GFAP (1:1000
587    dilution, AbCam; ab4674). Then we performed secondary antibody staining for 2.5 hours
588    using Donkey x Chicken Dig-MA-NHS (prepared in our lab). After immunostaining, we
589    performed anchoring for 10 minutes using 0.25% glutaraldehyde solution. Tissue sample
590    was gelated, stained and expanded in a similar way to the Label-Retention expansion
591    microscopy[34, 41]. All reactions are done at room temperature, and after each step sample
592    was washed for 3 times in PBS (unless it is specified otherwise).

593    **Protein anchoring, gelation, denaturation, post-digestion fluorescent staining, and**
594    **expansion steps of the x4 PL-ExM**

595    Protein anchoring: After PL and immunostaining of the samples, one of the three
596    anchoring reagents has been used:  0.25% Glutaraldehyde (GA; Electron Microscopy
597    Sciences; 16120) solution prepared in PBS for 10-minute room temperature incubation,
598    25mM Methacrylic acid N-hydroxysuccinimide ester (MA-NHS; Simga-Aldrich; 730300)
599    solution prepared in PBS for 1-hour room temperature incubation or 0.04% glycidyl
600    methacrylate solution prepared in 100mM sodium bicarbonate, pH 8.5 (GMA; Sigma-
601    Aldrich; 151238) for 4-hour room temperature incubation. The three anchoring reagents
602    yielded similar anchoring efficiency.

603    Gelation, denaturation, fluorescent staining, and expansion have been performed in a
604    similar way to the Label-Retention expansion microscopy (LR-ExM) [34, 41]. Here we
605    describe the procedure briefly.

606    Gelation: The samples were first incubated with monomer solution (8.6 g sodium acrylate,
607    2.5 g acrylamide, 0.15 g N,N'-methylenebisacrylamide (bis), 11.7 g sodium chloride in
608    100 ml PBS buffer) on ice for 5 min. Gelation solution (mixture of monomer solution, 10%
609    (w/v)  N,N,N',N' Tetramethylethylenediamine (TEMED) stock solution, 10% (w/v)
610    ammonium persulfate (APS) stock solution and water at 47:1:1:1 volume ratio) was then
611    quickly added to the samples and incubated on ice for another 5 min. The samples with
612    gelation solution were later transferred to a 37 °C humidity chamber for gelation for 2
613    hours.

614 Denaturation: After 1 h gelation, the gelated samples were immersed in proteinase K
615 buffer (8 units/mL proteinase K in digestion buffer made of 50 mM Tris pH 8.0, 1 mM
616 EDTA, 0.5% Triton X-100, 1M NaCl), and then washed with excess of DNase/RNase-free
617 water. For cultured cells, the proteinase K incubation duration was 16 hours at room
618 temperature. For tissues, the duration was 1.5 hours at 78°C.

619 Post-digestion fluorescent staining: The gelated samples were incubated in a mixture of
620 3 uM fluorescently labeled streptavidin (e.g. streptavidin-Alexa Fluor 488) and
621 fluorescently labeled anti-DIG antibodies (e.g. anti-DIG-DyLight 594) buffer for 24 hours
622 at room temperature. The staining buffer comprises 10 mM HEPES and 150 mM NaCl in
623 water at pH 7.5.
624
625 Expansion: The gelated samples were expanded in DNase/RNase-free water for more
626 than 4 hours at room temperature. Fully expanded gelated samples were trimmed and
627 transferred to a poly-lysine-coated glass bottom multiwell plate or dish for imaging.

628 **Protein anchoring, gelation, denaturation, post-digestion fluorescent staining, and**
629 **expansion steps of the x8 PL-ExM**

630 The anchoring, digestion, and post-digestion fluorescent staining steps of the x8 PL-ExM
631 were identical to those of the x4 PL-ExM. The gel monomer recipe and expansion steps
632 of the 8x PL-ExM were modified based on the TREx protocol[38]. Briefly, the samples were
633 first incubated with monomer solution for x8 expansion (1.1 M sodium acrylate, 2.0 M
634 acrylamide, 50 ppm bis in PBS) on ice for 5 min. Gelation solution (mixture of monomer
635 solution,1.5 ppt APS, and 1.5 ppt TEMED) was then quickly added to the samples and
636 incubated on ice for another 5 min. The samples with gelation solution were later
637 transferred to a 37 °C humidity chamber for gelation for 2 hours. The expansion step was
638 similar to that of the x4 PL-ExM except for the overnight expansion duration at room
639 temperature.
640
641 **Image acquisition and analysis**

642 Airyscan imaging for PL-ExM data was performed on Zeiss LSM 980 and Zeiss LSM 900
643 with a 63x water immersion objective (Zeiss Plan Apo 63x NA 1.15). Non-expanded
644 samples were imaged with Airyscan mode using Zeiss LSM 980 with a 63x water
645 immersion objective (Zeiss Plan Apo 63x NA 1.15). Confocal imaging was performed on
646 either Zeiss LSM 980 using 63x water immersion objective (Zeiss Plan Apo 63x NA 1.15)
647 or a spinning-disk confocal microscope (Nikon CSU-W1 Sora) with a 40× water-
648 immersion objective (Nikon CFI Apo 40× WI NA 1.15). The fluorescence intensity of
649 Airyscan and confocal images was analyzed using the open-source software Fiji
650 (ImageJ). No deconvolution was applied to any images in this work.

651 **Image intensity quantitative analysis and statistics**

652 Images were first denoised where we define a noise such as

653
$$Noise = 0.1 * (Intensity_{max} - Intensity_{min})$$

654  We use Matlab improfile function to select the cross-sectional area of proximity labeled
655  diameter and fit the Gaussian function and measure the full width half maximum (FWHM)
656  from it. We used single-slice images to measure the FWHM. Customized Matlab codes
657  were used, and the codes are available upon request. The mean and a standard error
658  were obtained from >=90 measurements across 3 independent samples. For Figure 4,
659  student t-test was performed to calculate p-value and determine statistical significance.

**Protein purification and digestion for MS**

661  The cell pellets were lysed in lysis buffer [50 mM Tris-HCl, 500 mM NaCl, 0.2% SDS, 1%
662  Triton, 1 mM Tris(2-carboxyethyl) phosphine hydrochloride (TCEP), 10 mM sodium azide,
663  10 mM sodium ascorbate, 5 mM TROLOX, protease inhibitor cocktail (pH 7.5)] with
664  sonication on ice. The lysates were centrifuged at 13, 000 rpm for 15 minutes to remove
665  cell debris, and the supernatant was incubated with streptavidin Mag Sepharose resin
666  (Cytiva) for overnight at 4°C with rotation. The streptavidin beads were then washed twice
667  with four buffers containing: A) 2% SDS at room temperature; B) 50 mM Tris-HCl, 500
668  mM NaCl, 2% Triton-X; C) 50 mM Tris-HCl, 250 mM NaCl, 0.5% SDS, 0.5% Triton-X and
669  D) 2 M Urea, 50 mM Tris-HCl at 4 °C. The bound proteins were then reduced, alkylated,
670  and digested on-bead by LysC in 8M urea/25mM $NH_4HCO_3$ for 4 hours, followed by
671  trypsin in 1.5 M urea/25 $NH_4HCO_3$ overnight at 37°C. The peptide digests were extracted
672  and desalted with C18 tip (Agilent) prior to liquid chromatography tandem mass
673  spectrometry (LC MS/MS)[54].

**Mass spectrometry analysis**

675  The peptide digests were subjected to LC MS/MS analysis using an UltiMate 3000 RSLC
676  system (Thermo Fisher Scientific) coupled in-line to an Orbitrap Fusion Lumos mass
677  spectrometer (Thermo Fisher Scientific). Reverse-phase separation was performed on a
678  50 cm x 75 μm I.D. Acclaim® PepMap RSLC column. Peptides were eluted using a
679  gradient of 4% to 22% B over 87 minutes at a flow rate of 300 nL/min (solvent A: 100%
680  H2O, 0.1% formic acid; solvent B: 100% acetonitrile, 0.1% formic acid). Each cycle
681  consisted of one full Fourier transform scan mass spectrum (375–1500 m/z, resolution of
682  120,000 at m/z 400) followed by data-dependent MS/MS scans acquired in the Orbitrap
683  with HCD NCE 30% at top speed for 3 seconds. Target ions already selected for MS/MS
684  were dynamically excluded for 30s. Protein identification and label-free quantitation was
685  carried out using MaxQuant as described [55]. Raw spectrometric files were searched
686  using MaxQuant (v. 2.0.3.0) against a FASTA of the complete human proteome obtained
687  from SwissProt (version from April 2023). The first search peptide tolerance was set to 15
688  ppm, with main search peptide tolerance set to 4.5 ppm. Trypsin was set as the digestive
689  enzyme with max 2 missed cleavages. Methionine oxidation and protein N-terminal
690  acetylation were set as variable modifications, while cysteine carbamidomethylation was
691  set as a fixed modification. Peptide spectra match and protein FDRs were both set as
692  0.01. For quantitation, intensities were determined as the full peak volume over the
693  retention time profile. "Unique plus razor peptides" was selected as the degree of
694  uniqueness required for peptides to be included in quantification. The resulting iBAQ
695  values for each identified protein by MaxQuant were used for comparing protein relative
696  abundances. For figure 3O-R, we performed two mass spectrometry experiments to make
697  a quantitative comparison between PL performed on U2OS cells overexpressing APEX2-

698 OMM vs PL performed on U2OS which has TOMM20 immunostained with HRP-
699 conjugated antibodies. For each condition, we also included negative controls. First, we
700 cultured both U2OS-*APEX2-OMM* (experimental, and negative control) and WT U2OS
701 cells (experimental, and negative control) in multiple 150 mm dishes, trypsinized cells,
702 and collected them into 1.5 mL Eppendorf tube after centrifugation at 1800 rpm for 3
703 minutes. Final counts used for each condition was about $2*10^8$ cells per condition. In
704 figure 3O,Q,R, U2OS-*APEX2-OMM* cells were used. We treated both experimental and
705 control conditions using 500μL of 1mM Bitoin Phenol solution (BP, in PBS) at 37°C for 2
706 hours. Without removing BP solution, the experimental condition was treated with the
707 same volume of 2mM freshly prepared $H_2O_2$ solution for 1 minute, followed by the addition
708 of 750μL of 15mM sodium ascorbate solution for reaction quenching. The sample was
709 thoroughly washed using PBS for 2 times with each 3 minute interval. After the proximity
710 labeling step, each sample was fixed with 1% paraformaldehyde (PFA) solution; the
711 control condition was immediately fixed with freshly prepared 1% paraformaldehyde
712 (PFA) after BP incubation (but no $H_2O_2$ treatment). After every step, we thoroughly
713 homogenize the sample, and centrifuge the sample at 500G for 3 minutes to pallet the
714 sample before next treatment. In figure 3P-R, WT U2OS cells were used. Cells were first
715 fixed with 0.1 % glutaraldehyde (GA) for 15 minutes at room temperature, and then
716 washed with PBS 3minutes for 3 times. We incubated cells with blocking buffer (3% BSA
717 in PBS) for 30 minutes and performed primary antibody staining using Rabbit x TOMM20
718 (1:250 dilution, santa cruz; sc-11415) overnight at 4°C. After washing samples 3 times
719 using blocking buffer (5 minute each), we stained samples with 3μg/mL AffiniPure Goat x
720 Rabbit (1:100, Jackson ImmunoResearch; 111-005-144) in blocking buffer for 1hour at
721 room temperature, then washed with blocking buffer three times (5 minute each). We then
722 stained samples with Goat-HRP (no dilution, Vector Laboratories; MP-7405) for 1hour at
723 room temperature, washed with blocking buffer 3 times for 5 minutes each. Next, we
724 incubated cells in 500μL of 0.5mM BP solution at RT for 15 minutes. We stopped any
725 further treatment to negative control at this step; meanwhile, the experimental condition
726 was treated with 500μL of 2mM $H_2O_2$ solution for 30 seconds at room temperature,
727 followed by the addition of 750μL sodium ascorbate solution. After 5 minute of incubation,
728 samples were thoroughly washed with PBS 3 times.

729 **Image resolution measurement**

730 0.1μm size fluorescent beads (TetraSpeck Microspheres, Invitrogen; T7279) were used
731 to measure the resolution of the Airyscan LSM980 resolution with 63x water immersion
732 objective (NA1.15). 30 different beads were sampled to obtain the average full width half
733 maximum (FWHM) with standard error. Effective resolution of PL-ExM was measured by
734 calculating FWHM divided by the physical expansion factor of the hydrogel.

735

736 **AUTHOR CONTRIBUTIONS**
737 S.P. and X.S. conceived and led the research. S.P. performed PL-ExM, imaging, and
738 prepared samples for MS analysis. X.W. performed MS experiments and analysis. X.L.
739 and X.S. initialized the concept and performed preliminary experiments. X. H. made
740 plasmids, and generated cell lines with X. S. K.F. performed cell experiments under S.P.

supervision. A.A.T synthesized early versions of LR-ExM probes. Z.D. synthesized LR-ExM probes. L.S. assisted Airyscan imaging. L.H. led and supervised MS work. X.W performed MS experiments. X.W., C.Y and L.H analyzed MS data. K.F assisted sample preparation. S.P, X.S, and L,H. drafted and edited the manuscript.

**Notes**

The authors declare no competing financial interest.

# REFERENCES

1.      Geri, J. B.; Oakley, J. V.; Reyes-Robles, T.; Wang, T.; McCarver, S. J.; White, C. H.; Rodriguez-Rivera, F. P.; Parker, D. L., Jr.; Hett, E. C.; Fadeyi, O. O.; Oslund, R. C.; MacMillan, D. W. C., Microenvironment mapping via Dexter energy transfer on immune cells. *Science* **2020,** *367* (6482), 1091-1097.

2.      Killinger, B. A.; Marshall, L. L.; Chatterjee, D.; Chu, Y.; Bras, J.; Guerreiro, R.; Kordower, J. H., In situ proximity labeling identifies Lewy pathology molecular interactions in the human brain. *Proc Natl Acad Sci U S A* **2022,** *119* (5).

3.      Uezu, A.; Kanak, D. J.; Bradshaw, T. W. A.; Soderblom, E. J.; Catavero, C. M.; Burette, A. C.; Weinberg, R. J.; Soderling, S. H., Identification of an elaborate complex mediating postsynaptic inhibition. *Science* **2016,** *353* (6304), 1123-1129.

4.      Takano, T.; Wallace, J. T.; Baldwin, K. T.; Purkey, A. M.; Uezu, A.; Courtland, J. L.; Soderblom, E. J.; Shimogori, T.; Maness, P. F.; Eroglu, C.; Soderling, S. H., Chemico-genetic discovery of astrocytic control of inhibition in vivo. *Nature* **2020,** *588* (7837).

5.      Kwon, Y.; Mehta, S.; Clark, M.; Walters, G.; Zhong, Y.; Lee, H. N.; Sunahara, R. K.; Zhang, J., Non-canonical beta-adrenergic activation of ERK at endosomes. *Nature* **2022,** *611* (7934), 173-179.

6.      Kotani, N.; Gu, J.; Isaji, T.; Udaka, K.; Taniguchi, N.; Honke, K., Biochemical visualization of cell surface molecular clustering in living cells. *Proc Natl Acad Sci U S A* **2008,** *105* (21), 7405-9.

7.      Honke, K.; Kotani, N., Identification of cell-surface molecular interactions under living conditions by using the enzyme-mediated activation of radical sources (EMARS) method. *Sensors (Basel)* **2012,** *12* (12), 16037-45.

8.      Jiang, S.; Kotani, N.; Ohnishi, T.; Miyagawa-Yamguchi, A.; Tsuda, M.; Yamashita, R.; Ishiura, Y.; Honke, K., A proteomics approach to the cell-surface interactome using the enzyme-mediated activation of radical sources reaction. *Proteomics* **2012,** *12* (1), 54-62.

782    9.      Martell, J. D.; Deerinck, T. J.; Sancak, Y.; Poulos, T. L.; Mootha, V. K.; Sosinsky,
783    G. E.; Ellisman, M. H.; Ting, A. Y., Engineered ascorbate peroxidase as a genetically encoded
784    reporter for electron microscopy. *Nature Biotechnology* **2012,** *30* (11), 1143-+.
785    10.     Hung, V.; Zou, P.; Rhee, H. W.; Udeshi, N. D.; Cracan, V.; Svinkina, T.; Carr, S.
786    A.;   Mootha, V. K.; Ting, A. Y., Proteomic Mapping of the Human Mitochondrial
787    Intermembrane Space in Live Cells via Ratiometric APEX Tagging. *Mol Cell* **2014,** *55* (2),
788    332-341.
789    11.     Lam, S. S.; Martell, J. D.; Kamer, K. J.; Deerinck, T. J.; Ellisman, M. H.; Mootha,
790    V. K.; Ting, A. Y., Directed evolution of APEX2 for electron microscopy and proximity
791    labeling. *Nat Methods* **2015,** *12* (1), 51-4.
792    12.     Roux, K. J.; Kim, D. I.; Raida, M.; Burke, B., A promiscuous biotin ligase fusion
793    protein identifies proximal and interacting proteins in mammalian cells. *Journal of Cell Biology*
794    **2012,** *196* (6), 801-810.
795    13.     Kim, D. I.; Jensen, S. C.; Noble, K. A.; Kc, B.; Roux, K. H.; Motamedchaboki, K.;
796    Roux, K. J., An improved smaller biotin ligase for BioID proximity labeling. *Mol Biol Cell*
797    **2016,** *27* (8), 1188-96.
798    14.     Go, C. D.; Knight, J. D. R.; Rajasekharan, A.; Rathod, B.; Hesketh, G. G.; Abe,
799    K. T.; Youn, J. Y.; Samavarchi-Tehrani, P.; Zhang, H.; Zhu, L. Y.; Popiel, E.; Lambert,
800    J. P.; Coyaud, E.; Cheung, S. W. T.; Rajendran, D.; Wong, C. J.; Antonicka, H.; Pelletier,
801    L.; Palazzo, A. F.; Shoubridge, E. A.; Raught, B.; Gingras, A. C., A proximity-dependent
802    biotinylation map of a human cell. *Nature* **2021,** *595* (7865), 120-+.
803    15.     Mair, A.; Xu, S. L.; Branon, T. C.; Ting, A. Y.; Bergmann, D. C., Proximity labeling
804    of protein complexes and cell-type-specific organellar proteomes in Arabidopsis enabled by
805    TurboID. *Elife* **2019,** *8*.
806    16.     Cho, K. F.; Branon, T. C.; Udeshi, N. D.; Myers, S. A.; Carr, S. A.; Ting, A. Y.,
807    Proximity labeling in mammalian cells with TurboID and split-TurboID. *Nat Protoc* **2020,** *15*
808    (12), 3971-3999.
809    17.     Hwang, J.; Ribbens, D.; Raychaudhuri, S.; Cairns, L.; Gu, H.; Frost, A.; Urban, S.;
810    Espenshade, P. J., A Golgi rhomboid protease Rbd2 recruits Cdc48 to cleave yeast SREBP.
811    *EMBO J* **2016,** *35* (21), 2332-2349.
812    18.     Gingras, A. C.; Abe, K. T.; Raught, B., Getting to know the neighborhood: using
813    proximity-dependent biotinylation to characterize protein complexes and map organelles. *Curr*
814    *Opin Chem Biol* **2019,** *48*, 44-54.
815    19.     Zuzow, N.; Ghosh, A.; Leonard, M.; Liao, J.; Yang, B.; Bennett, E. J., Mapping the
816    mammalian ribosome quality control complex interactome using proximity labeling
817    approaches. *Mol Biol Cell* **2018,** *29* (10), 1258-1269.
818    20.     Lobingier, B. T.; Huttenhain, R.; Eichel, K.; Miller, K. B.; Ting, A. Y.; von Zastrow,
819    M.; Krogan, N. J., An Approach to Spatiotemporally Resolve Protein Interaction Networks in
820    Living Cells. *Cell* **2017,** *169* (2), 350-360 e12.
821    21.     Chen, F.; Tillberg, P. W.; Boyden, E. S., Expansion microscopy. *Science* **2015,** *347*
822    (6221), 543-548.
823    22.     Chen, F.; Tillberg, P. W.; Boyden, E. S., Expansion microscopy. *Science* **2015,** *347*
824    (6221).

825  23.    Chozinski, T. J.; Halpern, A. R.; Okawa, H.; Kim, H. J.; Tremel, G. J.; Wong, R.
826  O.; Vaughan, J. C., Expansion microscopy with conventional antibodies and fluorescent
827  proteins. *Nat Methods* **2016,** *13* (6), 485-8.
828  24.    Tillberg, P. W.; Chen, F.; Piatkevich, K. D.; Zhao, Y.; Yu, C. C.; English, B. P.;
829  Gao, L.; Martorell, A.; Suk, H. J.; Yoshida, F.; DeGennaro, E. M.; Roossien, D. H.; Gong,
830  G.; Seneviratne, U.; Tannenbaum, S. R.; Desimone, R.; Cai, D.; Boyden, E. S., Protein-
831  retention expansion microscopy of cells and tissues labeled using standard fluorescent proteins
832  and antibodies. *Nat Biotechnol* **2016,** *34* (9), 987-92.
833  25.    Mao, C. Y.; Lee, M. Y.; Jhan, J. R.; Halpern, A. R.; Woodworth, M. A.; Glaser,
834  A. K.; Chozinski, T. J.; Shin, L.; Pippin, J. W.; Shankland, S. J.; Liu, J. T.; Vaughan, J.
835  C., Feature-rich covalent stains for super-resolution and cleared tissue fluorescence microscopy.
836  *Sci Adv* **2020,** *6* (22).
837  26.    M'Saad, O.; Bewersdorf, J., Light microscopy of proteins in their ultrastructural context.
838  *Nat Commun* **2020,** *11* (1), 3850.
839  27.    Pownall, M. E.; Miao, L. Y.; Vejnar, C. E.; M'Saad, O.; Sherrard, A.; Frederick,
840  M. A.; Benitez, M. D. J.; Boswell, C. W.; Zaret, K. S.; Bewersdorf, J.; Giraldez, A. J.,
841  Chromatin expansion microscopy reveals nanoscale organization of transcription and
842  chromatin. *Science* **2023,** *381* (6653), 92-99.
843  28.    Klimas, A.; Gallagher, B. R.; Wijesekara, P.; Fekir, S.; DiBernardo, E. F.; Cheng,
844  Z.; Stolz, D. B.; Cambi, F.; Watkins, S. C.; Brody, S. L.; Horani, A.; Barth, A. L.; Moore,
845  C. I.; Ren, X.; Zhao, Y., Magnify is a universal molecular anchoring strategy for expansion
846  microscopy. *Nat Biotechnol* **2023,** *41* (6), 858-869.
847  29.    Sun, D. E.; Fan, X.; Shi, Y.; Zhang, H.; Huang, Z.; Cheng, B.; Tang, Q.; Li, W.;
848  Zhu, Y.; Bai, J.; Liu, W.; Li, Y.; Wang, X.; Lei, X.; Chen, X., Click-ExM enables expansion
849  microscopy for all biomolecules. *Nat Methods* **2021,** *18* (1), 107-113.
850  30.    Wang, U.-T. T.; Tian, X.; Liou, Y.-H.; Lee, S.-P.; Lu, C.-H.; Chen, P.; Cheb, B.-
851  C., Expansion microscopy with trypsin digestion and tyramide signal amplification (TT-ExM)
852  for protein and lipid staining. *bioRxiv* **2023**.
853  31.    Qin, W.; Cho, K. F.; Cavanagh, P. E.; Ting, A. Y., Deciphering molecular interactions
854  by proximity labeling. *Nature Methods* **2021,** *18* (2), 133-143.
855  32.    Oakley, J. V.; Buksh, B. F.; Fernandez, D. F.; Oblinsky, D. G.; Seath, C. P.; Geri,
856  J. B.; Scholes, G. D.; MacMillan, D. W. C., Radius measurement via super-resolution
857  microscopy enables the development of a variable radii proximity labeling platform. *Proc Natl
858  Acad Sci U S A* **2022,** *119* (32), e2203027119.
859  33.    Chen, F.; Tillberg, P. W.; Boyden, E. S., Optical imaging. Expansion microscopy.
860  *Science* **2015,** *347* (6221), 543-8.
861  34.    Shi, X.; Li, Q.; Dai, Z.; Tran, A. A.; Feng, S.; Ramirez, A. D.; Lin, Z.; Wang, X.;
862  Chow, T. T.; Chen, J.; Kumar, D.; McColloch, A. R.; Reiter, J. F.; Huang, E. J.; Seiple,
863  I. B.; Huang, B., Label-retention expansion microscopy. *J Cell Biol* **2021,** *220* (9).
864  35.    Truckenbrodt, S.; Maidorn, M.; Crzan, D.; Wildhagen, H.; Kabatas, S.; Rizzoli, S.
865  O., X10 expansion microscopy enables 25-nm resolution on conventional microscopes. *EMBO
866  Rep* **2018,** *19* (9).
867  36.    Truckenbrodt, S.; Sommer, C.; Rizzoli, S. O.; Danzl, J. G., A practical guide to
868  optimization in X10 expansion microscopy. *Nat Protoc* **2019,** *14* (3), 832-863.

37.     Park, H. E.; Choi, D.; Park, J. S.; Sim, C.; Park, S.; Kang, S.; Yim, H.; Lee, M.; Kim, J.; Pac, J.; Rhee, K.; Lee, J.; Lee, Y.; Lee, Y.; Kim, S. Y., Scalable and Isotropic Expansion of Tissues with Simply Tunable Expansion Ratio. *Adv Sci (Weinh)* **2019,** *6* (22), 1901673.

38.     Damstra, H. G. J.; Mohar, B.; Eddison, M.; Akhmanova, A.; Kapitein, L. C.; Tillberg, P. W., Visualizing cellular and tissue ultrastructure using Ten-fold Robust Expansion Microscopy (TREx). *Elife* **2022,** *11.*

39.     Saal, K. A.; Shaib, A. H.; Mougios, N.; Crzan, D.; Opazo, F.; Rizzoli, S. O., Heat denaturation enables multicolor X10-STED microscopy. *Sci Rep* **2023,** *13* (1), 5366.

40.     Chang, J. B.; Chen, F.; Yoon, Y. G.; Jung, E. E.; Babcock, H.; Kang, J. S.; Asano, S.; Suk, H. J.; Pak, N.; Tillberg, P. W.; Wassie, A. T.; Cai, D.; Boyden, E. S., Iterative expansion microscopy. *Nat Methods* **2017,** *14* (6), 593-599.

41.     Park, S.; Zhuang, Y.; Shi, X., Label-Retention Expansion Microscopy (LR-ExM) Enables Super-Resolution Imaging and High-Efficiency Labeling. *J Vis Exp* **2022,** (188).

42.     Zhuang, Y. Y.; Shi, X. Y., Expansion microscopy: A chemical approach for super-resolution microscopy. *Curr Opin Struc Biol* **2023,** *81.*

43.     Montagnac, G.; Meas-Yedid, V.; Irondelle, M.; Castro-Castro, A.; Franco, M.; Shida, T.; Nachury, M. V.; Benmerah, A.; Olivo-Marin, J. C.; Chavrier, P., alphaTAT1 catalyses microtubule acetylation at clathrin-coated pits. *Nature* **2013,** *502* (7472), 567-70.

44.     Guo, Y. T.; Li, D.; Zhang, S. W.; Yang, Y. R.; Liu, J. J.; Wang, X. Y.; Liu, C.; Milkie, D. E.; Moore, R. P.; Tulu, U. S.; Kiehart, D. P.; Hu, J. J.; Lippincott-Schwartz, J.; Betzig, E.; Li, D., Visualizing Intracellular Organelle and Cytoskeletal Interactions at Nanoscale Resolution on Millisecond Timescales. *Cell* **2018,** *175* (5), 1430-+.

45.     Mick, D. U.; Rodrigues, R. B.; Leib, R. D.; Adams, C. M.; Chien, A. S.; Gygi, S. P.; Nachury, M. V., Proteomics of Primary Cilia by Proximity Labeling. *Dev Cell* **2015,** *35* (4), 497-512.

46.     Kang, M. G.; Rhee, H. W., Molecular Spatiomics by Proximity Labeling. *Acc Chem Res* **2022,** *55* (10), 1411-1422.

47.     Hung, V.; Udeshi, N. D.; Lam, S. S.; Loh, K. H.; Cox, K. J.; Pedram, K.; Carr, S. A.; Ting, A. Y., Spatially resolved proteomic mapping in living cells with the engineered peroxidase APEX2. *Nat Protoc* **2016,** *11* (3), 456-75.

48.     Chung, K.; Wallace, J.; Kim, S. Y.; Kalyanasundaram, S.; Andalman, A. S.; Davidson, T. J.; Mirzabekov, J. J.; Zalocusky, K. A.; Mattis, J.; Denisin, A. K.; Pak, S.; Bernstein, H.; Ramakrishnan, C.; Grosenick, L.; Gradinaru, V.; Deisseroth, K., Structural and molecular interrogation of intact biological systems. *Nature* **2013,** *497* (7449), 332-+.

49.     Gambarotto, D.; Zwettler, F. U.; Le Guennec, M.; Schmidt-Cernohorska, M.; Fortun, D.; Borgers, S.; Heine, J.; Schloetel, J. G.; Reuss, M.; Unser, M.; Boyden, E. S.; Sauer, M.; Hamel, V.; Guichard, P., Imaging cellular ultrastructures using expansion microscopy (U-ExM). *Nat Methods* **2019,** *16* (1), 71-74.

50.     Kubalová, I.; Cernohorská, M. S.; Huranová, M.; Weisshart, K.; Houben, A.; Schubert, V., Prospects and limitations of expansion microscopy in chromatin ultrastructure determination. *Chromosome Res* **2020,** *28* (3-4), 355-368.

51.     Bourguignon, L. Y., Biochemical analysis of ligand-induced receptor patching and capping using a novel immunolactoperoxidase iodination technique. *J Cell Biol* **1979,** *83* (3), 649-56.

914   52.    Szklarczyk, D.; Gable, A. L.; Lyon, D.; Junge, A.; Wyder, S.; Huerta-Cepas, J.;
915   Simonovic, M.; Doncheva, N. T.; Morris, J. H.; Bork, P.; Jensen, L. J.; Mering, C. V.,
916   STRING v11: protein-protein association networks with increased coverage, supporting
917   functional discovery in genome-wide experimental datasets. *Nucleic Acids Res* **2019,** *47* (D1),
918   D607-D613.
919   53.    Saka, S. K.; Wang, Y.; Kishi, J. Y.; Zhu, A.; Zeng, Y.; Xie, W.; Kirli, K.; Yapp,
920   C.; Cicconet, M.; Beliveau, B. J.; Lapan, S. W.; Yin, S.; Lin, M.; Boyden, E. S.; Kaeser,
921   P. S.; Pihan, G.; Church, G. M.; Yin, P., Immuno-SABER enables highly multiplexed and
922   amplified protein imaging in tissues. *Nat Biotechnol* **2019,** *37* (9), 1080-1090.
923   54.    Yu, C.; Yang, Y. Y.; Wang, X. R.; Guan, S. H.; Fang, L.; Liu, F.; Walters, K. J.;
924   Kaiser, P.; Huang, L., Characterization of Dynamic UbR-Proteasome Subcomplexes by In vivo
925   Cross-linking (X) Assisted Bimolecular Tandem Affinity Purification (XBAP) and Label-free
926   Quantitation. *Mol Cell Proteomics* **2016,** *15* (7), 2279-2292.
927   55.    Cox, J.; Mann, M., MaxQuant enables high peptide identification rates, individualized
928   p.p.b.-range mass accuracies and proteome-wide protein quantification. *Nature Biotechnology*
929   **2008,** *26* (12), 1367-1372.

930